Inorganica Chimica Acta 483 (2018) 454–463

Contents lists available at ScienceDirect

Inorganica Chimica Acta

journal homepage: www.elsevier.com/locate/ica

Research paper

# Metallo-supramolecular assemblies of dinuclear Zn(II) and Mn(II) secondary building units (SBUs) and a bent silicon dicarboxylate ligand

Georgiana-Oana Turcan-Trofin, Mihaela Avadanei, Sergiu Shova, Angelica Vlad, Maria Cazacu, Mirela-Fernanda Zaltariov*

*"Petru Poni" Institute of Macromolecular Chemistry, Aleea Gr. Ghica Voda 41A, 700487 Iasi, Romania*

ARTICLE INFO

*Keywords:*
Metallo-supramolecular polymer
Paddle-wheel clusters
Silicon-containing dicarboxylic acid
X-ray single crystal diffraction
Luminescence properties

ABSTRACT

Two metallo-supramolecular polymers $\{[Zn_2(L)_4(DMF)_2]\cdot 0.8DMF\}_n$ (1) and $\{[Mn_2L_2(DMSO)_4]\cdot 2DMSO\}_n$ (2) ($H_2L$ = bis(*p*-carboxyphenyl)diphenylsilane) have been synthetized by the reaction of $Zn(NO_3)_2\cdot 6H_2O$ and $Mn(NO_3)_2\cdot 4H_2O$ respectively, with the above mentioned acid as ligand under solvothermal conditions. Both coordination polymers were structurally characterized by single crystal X-ray diffraction, elemental analysis, FTIR and UV–Vis spectroscopy. Single crystal X-ray diffraction analysis reveals dinuclear Zn(II) and Mn(II) nodes bridged by mono or double deprotonated ligand molecules coordinated in *syn-syn* bidentate mode. Thermal and moisture stability and photophysical properties of the resulting coordination polymers were studied and correlated with their structure.

## 1. Introduction

Recently, the research in the field of advanced materials was directed to the synthesis of porous structures also called porous coordination polymers (PCPs) or metal-organic frameworks (MOFs) with applications in separation, heterogenous catalysis, gas storage, drug delivery, etc [1–13]. Coordination polymers (CPs) represent a new class of hybrid organic/inorganic materials formed by self-assembly of metallic ions or clusters with organic linkers. Compared to porous organic materials or their inorganic analogues (zeolites, silica), they have some unique advantages: 1) their design from synthesis (by choosing the appropriate metallic ions and organic linkers) which allows the adjustment not only of porosity, but also of the structure and chemical properties; 2) the possibility to vary their composition through chemical modifications or by selecting the proper component (ligands and metal ions) depending on the application field; 3) a high BET surface, larger pore size (up to 6 nm) and structural flexibility with a high potential for incorporation of different guest molecules [14].

The formation and the stability of CPs are mainly influenced by the nature and the number of the donor atoms in the structure of the ligands and the coordination geometry of the metal ions, as well as other physical factors: solvent nature, reaction temperature, pH value, counterions, reagents concentration, stoichiometry of the system, intermolecular interactions (H bonds and π-π stacking). The main advantage of these arises from the variety of the structural and chemical composition, which facilitates the design by chemical synthesis and allows optimizing the properties [14–17]. Polycarboxylic aromatic and aliphatic ones have been extensively used in the synthesis of a large number of structures ranging from 1D to 3D due to their ability to self-assembly through coordinative bonds and intermolecular interactions [18].

Coordination polymers built with aromatic rigid carboxylates prove to be porous which can be used in gas ($N_2$, $H_2$) sorption or $CO_2$ sequestration and in separation processes [19–21]. Beside these, flexible carboxylate ligands continue to occupy an enlarged significance [20,22,23].

Structural flexibility is a unique and interesting property especially for adsorption and selective separation (property difficult to achieve with rigid porous structures), and has a fundamental importance for luminescence, because the transient motion (vibration, torsion, etc.) of organic/inorganic luminophores at the excited state is the main cause of non-radiative relaxation of the excited-state energy [13]. In this context, luminescence-based chemical detection by CPs or MOFs has significant potential for developing sensitive and selective sensors for organic molecules (solvents, dyes, nitroaromatic derivatives), gas, cations, anions, or biomolecules [24]. In this work the structural characteristics (connectivity/porosity and hydrophobicity) induced by the presence in the structure of the synthesized CP of the silicon-containing carboxylate SBUs, were combined with the luminescent properties of the resulting structures, in order to achieve emissive devices with blue

* Corresponding author.
*E-mail address:* zaltariov.mirela@icmpp.ro (M.-F. Zaltariov).

https://doi.org/10.1016/j.ica.2018.08.027
Received 22 February 2018; Received in revised form 6 July 2018; Accepted 19 August 2018
Available online 20 August 2018
0020-1693/ 

emission (420 nm). When compared to their carbon analogues, the increased bond angle flexibility, decreased conformational rigidity and the longer bond lengths to silicon have been shown in some cases to contribute to the formation of novel topological CPs with various structural motifs, which are promising candidates for sensor applications [25–28].

There is a small number of publications in which silicon-containing carboxylic acids are used to prepare MOFs [29–31], all being structurally different from the one reported in this paper, built on the basis of *bis*(p-carboxyphenyl)diphenylsilane and Zn(II) or Mn(II) ions, by solvothermal method. The structural characterization, the fluorescence properties, thermal and moisture properties of $\{[Zn_2L_4(DMF)_2]\cdot 0.8DMF\}_n$ and $\{[Mn_2L_2(DMSO)_4]\cdot 2DMSO\}_n$ are investigated.

## 2. Experimental

### 2.1. Materials and measurements

Bis(*p*-carboxyphenyl)diphenylsilane was prepared according to Ref. [32], $Zn(NO_3)_2\cdot 6H_2O$, $Mn(NO_3)_2\cdot 4H_2O$ (Aldrich), dimethylformamide (DMF), dimethylsulfoxide (DMSO) (Aldrich), ethanol (Chimopar) and diethylether (Aldrich) were used as received.

Fourier transform infrared (FT-IR) spectra were recorded using a Bruker Vertex 70 FT-IR spectrometer. Registrations were performed in the transmission mode in the range 400–4000 $cm^{-1}$ at room temperature with a resolution of 2 $cm^{-1}$ and accumulation of 32 scans.

Elemental (C, H, N) analyses were obtained with a Perkin–Elmer CHNS 2400 II elemental analyser.

The UV–Vis absorption spectra were obtained in DMF solution on a Specord 200 spectrophotometer in a quartz cell with path length of 1.0 cm, and in solid state, using the diffuse reflectance accessory. Spectralon® was used as reference. The optical band gaps of the free ligand and compounds **1** and **2** were determined from the diffuse reflectance spectra.

Fluorescence spectra were obtained by using a Perkin Elmer LS55 luminescence spectrometer in solid state with integrating sphere and in DMF solution.

Dynamic water vapor sorption (DVS) capacity of the sample was determined in the relative humidity (RH) range 0–90% by using the fully automated gravimetric analyzer IGAsorp (Hiden Analytical, Warrington, UK). The sample previously dried at a constant weight at 25 °C in flowing nitrogen (250 mL/min) at RH < 1% was exposed to increasing humidity from 0 to 90%, in 10% humidity steps, each step having a pre-established equilibrium time between 5 and 10 min. When RH decreased, desorption curves were recorded.

Thermogravimetric (TG) curves and their corresponding first derivatives (DTG) were recorded on a STA 449 F1 Jupiter device (Netzsch, Germany). Around 10 mg of each sample was weighed and heated in alumina crucibles in nitrogen as inert atmosphere and at a flow rate of 50 mL $min^{-1}$. Samples were heated in the temperature range from 25 to 700 °C with a heating rate of 10 °C $min^{-1}$.

Differential scanning calorimetry (DSC) measurements were conducted on a DSC 200 F3 Maia (Netzsch, Germany). About 10 mg of sample were heated in pressed and punched aluminium crucibles at a heating rate of 10 °C/min. Nitrogen was used as inert atmosphere at a flow rate of 100 mL/min. A heating and cooling rate of 10 °C/min was applied.

The Energy Dispersive X-Ray system (EDX) of the SEM (Scanning Electron Microscope) was used for qualitative analysis of the residue obtained after the thermal decomposition of the samples. The residue was glued on carbon tape for this analysis.

### 2.2. X-ray crystallography

Crystallographic measurements for **1** and **2** were carried out with an Oxford-Diffraction XCALIBUR E CCD diffractometer equipped with graphite-monochromated Mo Kα radiation. Single crystals were positioned at 40 mm from the detector and 381 and 446 frames were measured each for 200 and 30 s over 1° scan width, respectively. The unit cell determination and data integration were carried out using the CrysAlis package of Oxford Diffraction [33]. The structures were solved by direct methods using Olex2 [34] software with the SHELXS structure solution program and refined by full-matrix least-squares on $F^2$ with SHELXL-97 [35]. Atomic displacements for non-hydrogen atoms were refined using an anisotropic model. Hydrogen atoms have been placed in fixed, idealized positions accounting for the hybridation of the supporting atoms. The positional parameters of the desordered fragments were refined in combination with AFIX, PART and SADI restrains using anisotropic/isotropic model for non-H atoms. The crystal **2** displayed a quite low diffraction quality with the resolution up to 1.1–1.2 Å. Consequently, the crystal structure refinement has resulted into a relatively high final value for $R_1$-factor (0.1147). Unfortunately, any attempt to select another crystal didn't improve the final parameters. The molecular plots were obtained using the Olex2 program. Table 1 provides a summary of the crystallographic data together with refinement details.

**Table 1**
Crystallographic data, details of data collection and structure refinement parameters for **1** and **2.**

| Empirical formula | $C_{60.4}H_{55.6}N_{2.8}O_{10.8}Si_2Zn_2$ | $C_{64}H_{76}Mn_2O_{15}S_6Si_2$ |
|---|---|---|
| Formula weight | 1180.449 | 1443.803 |
| Temperature/K | 160 | 200 |
| Crystal system | monoclinic | monoclinic |
| Space group | *C*2/*c* | $P2_1/c$ |
| *a*/Å | 13.3074(14) | 24.797(2) |
| *b*/Å | 42.600(5) | 10.0203(8) |
| *c*/Å | 10.8438(9) | 28.554(2) |
| *α*/° | 90.00 | 90.00 |
| *β*/° | 103.658(9) | 101.003(8) |
| γ/° | 90.00 | 90.00 |
| *V*/Å$^3$ | 5973.5(11) | 6964.5(9) |
| *Z* | 4 | 4 |
| $D_{calc}$/mg/mm$^3$ | 1.313 | 1.377 |
| $\mu$/mm$^{-1}$ | 0.902 | 0.639 |
| Crystal size/mm$^3$ | 0.10 × 0.05 × 0.05 | 0.45 × 0.15 × 0.08 |
| $\theta_{min,}\ \theta_{max}$(°) | 3.3–46.5 | 3.62–37.7 |
| Reflections collected | 17,128 | 22,118 |
| Independent reflections($R_{int}$) | 4288(0.0867) | 5449(0.0625) |
| Data/restraints/parameters | 4288/10/324 | 5449/47/820 |
| $R_1$[a]($I > 2\sigma(I)$) | 0.0883 | 0.1143 |
| $wR_2$[b](all data) | 0.2001 | 0.2625 |
| GOF[c] | 1.057 | 1.103 |
| Largest diff. peak/hole/e Å$^{-3}$ | 1.65/−0.80 | 1.44/−0.57 |

[a] $R_1 = \Sigma||F_o| - |F_c||/\Sigma|F_o|$.
[b] $wR_2 = \{\Sigma[w(F_o^2 - F_c^2)^2]/\Sigma[w(F_o^2)^2]\}^{1/2}$.
[c] GOF = $\{\Sigma[w(F_o^2 - F_c^2)^2]/(n-p)\}^{1/2}$, where *n* is the number of reflections and *p* is the total number of parameters refined.

CCDC-1476408 for **1** and 1509244 for **2** contain the supplementary crystallographic data for this contribution. These data can be obtained free of charge from the Cambridge Crystallographic Data Centre via www.ccdc.cam.ac.uk/data_request/cif.

### 2.3. Synthesis of the coordination polymers

#### 2.3.1. $\{[Zn_2(L)_4(DMF)_2]\cdot 0.8DMF\}_n$ (1)

Bis(*p*-carboxyphenyl)diphenylsilane (**$H_2$L**) (0.212 g, 0.5 mmol) was dissolved in DMF (8 mL). Separately $Zn(NO_3)\cdot 6H_2O$ (0.466 g, 1.5 mmol) was dissolved in DMF (2 mL) and then was added to bis(*p*-carboxyphenyl)diphenylsilane solution. The mixture was sonicated for 3 min and then was transferred into a 20 mL glass tube. The tube was entered into a Teflon-lined stainless steel vessel, heated at 125 °C for 72 h and then cooled slowly (1 °C/min) to room temperature. The resulting suspension was filtered off and the filtrate was evaporated at room

temperature. Colorless crystals were isolated after two weeks in a 36.11% yield (0.212 g). Anal. Calcd. for $C_{60.4}H_{55.6}N_{2.8}O_{10.8}Si_2Zn_2$ ($M_r$ 1180.449 g/mol): C, 61.46%; H, 4.75%; N, 3.32%. Found: C, 61.28%; H, 4.72%; N, 3.29%.

IR $\nu_{max}$ (KBr), $cm^{-1}$: 3431w, 3067w, 3049w, 2930w, 1676s, 1624vs, 1543m, 1497s, 1410, 1383s, 1254m, 1190m, 1107w, 1063w, 1001w, 845m, 773vs, 723m, 706m, 635m, 540w, 509w, 476vw, 430vw, 384vw.

#### 2.3.2. $\{[Mn_2L_2(DMSO)_4]\cdot 2DMSO\}_n$ (2)

A solution of bis(p-carboxyphenyl)diphenylsilane **($H_2L$)** (0.212 g, 0.5 mmol) in DMSO (8 mL) was dropwise added to a solution of Mn $(NO_3)_2\cdot 4H_2O$ (0.377 g, 1.40 mmol) in DMSO (2 mL). The mixture was sonicated for 3 min and transferred into a 20 mL glass tube. The tube was entered into a Teflon-lined stainless steel vessel, heated at 125 °C for 72 h and then cooled slowly (1 °C/min) to room temperature. The pale yellow precipitate was filtered off, and the filtrate was allowed to stand at room temperature. Yellow crystals appeared after three weeks.

Yield: 44.29% (0.318 g). Anal. Calcd. for $C_{64}H_{76}Mn_2O_{15}S_6Si_2$ (Mr 1443.803 g/mol): C, 53.24%; H, 5.31%; S, 13.33%. Found: C, 53.37%; H, 5.48%; S, 13.26%.

IR $\nu_{max}$ (KBr), $cm^{-1}$: 3439s, 3001, 2914w, 1622s, 1537m, 1491w, 1400vs, 1315w, 1157w, 1105m, 1020vs, 953s, 907w, 860vw, 826w, 773m, 746w, 716s, 554w, 534w, 509w, 476m, 407m.

## 3. Results and discussion

Reaction of bis(*p*-carboxyphenyl)diphenylsilane (**$H_2L$**) with Zn $(NO_3)\cdot 6H_2O$ and $Mn(NO_3)\cdot 4H_2O$, respectively, in 1:3 M ratio in solvothermal conditions (DMF or DMSO, 125 °C, 72 h) (Scheme 1) afforded colorless (1) and yellow (2) crystals after two or three weeks, respectively. The resulting coordination polymers are air stable and soluble in aprotic polar solvents: DMF and DMSO.

### 3.1. IR analysis

In the IR spectra of the obtained coordination polymers **1** and **2** the magnitude of the separation between the carboxylate asymmetric and symmetric stretches $\Delta = \upsilon_{as}(COO^-) - \upsilon_s(COO^-)$ was used to determine the mode of the carboxylate binding. Generally the following order is proposed for metal carboxylates: $\Delta_{(monodentate)} > \Delta_{(ionic)} > \Delta_{(bridging)} > \Delta_{(chelating)}$ [36].

In the IR spectrum of compound **1** the bands assigned to the carboxylate groups involved in coordination of the zinc ions are present at 1593 $cm^{-1}$ ($\upsilon_{as}$ $COO^-$) and 1426 $cm^{-1}$ ($\upsilon_s$ $COO^-$). The Δ value is 167 $cm^{-1}$ since $\Delta_{sodium\ salt}$ is 177 $cm^{-1}$, revealing the bidentate bridging coordination mode of the carboxylate groups in the Zn(II) coordination polymer (Figs. 1S(a) and S(b)).

For the compound **2** the $\upsilon_{as}(COO^-)$ and $\upsilon_s(COO^-)$ were observed at 1590 and 1428 $cm^{-1}$ proving the bridging mode of coordination of carboxylate groups to Mn(II) (Figs. 1S(c) and S(d)). Beside these the band at 1644 $cm^{-1}$ assigned to $\upsilon_{as}(COO^-)$ suggested that monodentate carboxylate coordination should be present in the compound **2**. The structural analysis has shown both coordination modes of the carboxylate groups: monodentate ($\Delta = 216\ cm^{-1} > \Delta_{sodium\ salt}$) and bidentate bridging ($\Delta = 162\ cm^{-1} < \Delta_{sodium\ salt}$). The bands at 1670 $cm^{-1}$ and 1662 $cm^{-1}$ in the 1700–1500 $cm^{-1}$ spectral region of **1** and **2**, respectively are assigned to the C=O vibration of the coordinated DMF molecules in the structure of **1** and to aqua bridged molecules in the structure of **2** (Figs. 1S(a) and S(c)).

The specific bands at for the diphenylsilane units can be observed at 1190 $cm^{-1}$ and 723 $cm^{-1}$ in **1** and at 1157 $cm^{-1}$ and 716 $cm^{-1}$ in **2**. The bands assigned to the C–H vibrations in aromatic rings can be seen at 3049 $cm^{-1}$ (1) and 3001 $cm^{-1}$ (2), while aromatic −C=C−C vibrations are present at 1624 $cm^{-1}$ (1) and 1622 $cm^{-1}$ (2). The newly formed bonds Zn-O and Mn-O are evidenced by the bands at 540 $cm^{-1}$ (Zn-O) and 554 $cm^{-1}$ (Mn-O) [37].

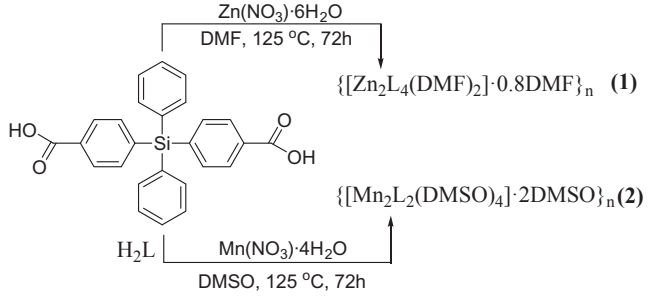


**Scheme 1.** Synthetic procedure for obtaining Zn(II) and Mn(II) coordination polymers.

### 3.2. X-ray crystallography

The result of single crystal X-ray study for **1** and **2**, along with atom numbering scheme, presented in Figs. 1 and 4, respectively. According to X-ray crystallography, the asymmetric part of the unit cell in **1** contains statistically distributed DMF as solvate molecules in general position with s.o.f. of 0.4. Thus, the composition of this compound are in agreement with the $[Zn_2L_4(DMF)_2]\cdot 0.8DMF$ species.

In the crystal the asymmetric units of **1** are self-assembled over the centers of symmetry to form one-dimensional polymeric chains, as shown in Fig. 2. The resulting coordination polymer is built up from dinuclear paddle-wheel nodes bridged by a pair of double deprotonated tetradentate bis(*p*-carboxyphenyl)diphenylsilane anions, where both carboxylate groups are coordinated in *syn-syn* bidentate mode. The two equivalent Zn atoms, separated at 2.941(2) Å, adopts a quite regular square-pyramidal environment coordinated equatorially to four carboxylate oxygen atoms (Zn-O 2.058(5) −2.060(5) Å) and apically to the oxygen atom of monodentate DMF molecule (Zn-O5 1.989(5) Å). The coordinated DMF was found to be disordered into two crystallographic independent positions with 1:1 probability.

In the crystal, the packing of coordination polymer chains occur with the formation of channels running parallel to *a* crystallographic axis (Fig. 3) accommodating solvate DMF molecules. These channels have the smallest and largest apertures of 8.9 Å and 11.3 Å, respectively, accommodating the coordination and solvate guest molecules of DMF.

The dinuclear fragment in compound **2** is constructed in a different way. The two manganese atoms separated at 3.729(3) Å are linked by two carboxylate groups fulfilling a *syn-syn* bidentate-bridging coordination mode with average Mn-O distance of 2.135(10) Å (Fig. 4). Another two carboxylate groups of double deprotonated tetradentate bis(*p*-carboxyphenyl)diphenylsilane anions are coordinated as monodentate ligands at Mn1-O11($x$, $0.5-y$, $-0.5+z$) 2.174(10) Å and Mn2-O12($x$, $0.5-y$, $0.5+z$) 2.180(10) Å distances (Fig. 4). Additionally, the dinuclear node is sustained by a μ-aqua-bridging molecule coordinated at 2.251(10) Å and 2.248(10) Å to Mn1 and Mn2, respectively. The hydrogen atoms of the water molecule act as donor of proton to the non-coordinated carboxylate oxygen atoms. As shown in Fig. 5, a similar 1D coordination polymer is formed in the crystal structure of **2**. The largest spherical void formed by the packing of the coordination polymers in the crystal (Fig. 6) doesn't exceed 17.2 $Å^3$.

### 3.3. Luminescence properties

CPs/MOFs research has shown that these compounds are highly efficient in gas storage and separation, while the research on luminescent MOFs is still at the early stage. Comprehensive experimental studies and screening the luminescence properties of those reported and future synthesized MOFs are still necessary to establish the updated

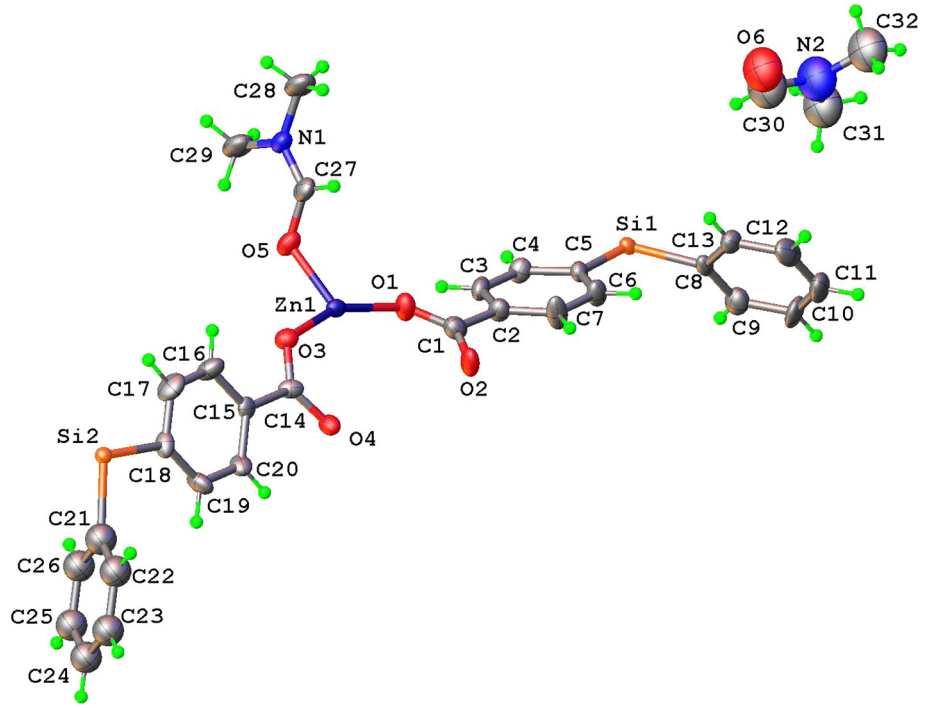


**Fig. 1.** View of the asymmetric part in the crystal structure of **1**. Thermal ellipsoids are drawn at 50% probability level.

database of luminescent MOFs. Their rational design is achieved by careful choice of organic ligands and by functionalizing them in order to increase the selectivity. Luminescent frameworks are by far the most widely explored type of sensor to date, their porous architecture providing advantages over other ones, while their structural and sorption properties offer a high degree of molecular specificity [26]. Based on the ISI Web of Science about 43,771 CPs have been reported in which 5223 of them are luminescent (about 12%), 794 are luminescent Zinc (II) CPs (1.8%), 94 are luminescent Manganese(II) CPs (0.2%) and only four results were found on luminescent CPs with silicon linkers. In contrast with those reported in the literature, the use of ligands containing diphenylsilane units in the structure is an original approach to design novel structures with conformational flexibility and hydrophobicity.

The photophysical properties of the ligand and of the CPs **1** and **2** were investigated in DMF solution and in solid state, by means of electronic absorption and emission spectroscopy.

The UV–Vis absorption spectrum (Figs. 1S(a) and S(c)) of the ligand **L** in DMF solution has very weak shoulders at 280 nm (ε = 5378 L/mol·cm), 288 nm (ε = 4176 L/mol·cm) and 308 nm (ε = 553 L/mol·cm) arising from the $\pi \rightarrow \pi^*$ and $\sigma \rightarrow \sigma^*$ transitions in the tetraphenylsilane core. Coordination led to a bathochromic shift in **1** and **2** to 300 nm and 308 nm, supplemented by development of a broad and very weak band around 390 nm in **1** and 360 nm in **2**, showing several maxima. The broad band can be assigned to ligand-centered absorption(in **1**) and ligand-to-metal (in **2**) charge transfer. The intense fluorescence of the ligand when excited with either 288 or 310 nm light (Fig. 7(a)) peaks at 340 nm and is arising from the excitation in the tetraphenylsilane fragment. **1** and **2** have similar fluorescence spectra that consist of two blue bands with maxima at 343 and 424 nm, and 370 and 402 nm, respectively. The violettish – blue emission is originating in the ligand-to-metal charge transfer, although the Zn(II) complexes usually display only the ligand-centered emission.

The DRS absorption spectra of the ligand and complexes extend into the visible region, The ligand show a new weak band around 480 nm, while **1** and **2** have more intense bands around 520 nm, and 440 and 580 nm, respectively. The overlapped and weak d-d transitions in the spectra of **2**, having a pyramidal geometry, have been spectrally resolved into $^4T_{1g}(G) \leftarrow {}^6A_{1g}$ (670 nm), $^4T_{2g}(G) \leftarrow {}^6A_{1g}$ (575 nm), $^4A_{1g}(G)$, $^4E_g(G) \leftarrow {}^6A_{1g}$ (448 nm), $^4T_{2g}(D) \leftarrow {}^6A_{1g}$ (398 nm) transitions [38,39], while the LMCT $d\pi(Mn(II)) \rightarrow \pi^*(L)$ band is seen at 355 nm. The crystal field parameters are B = 580 $cm^{-1}$ and C = 2778 $cm^{-1}$, and they are

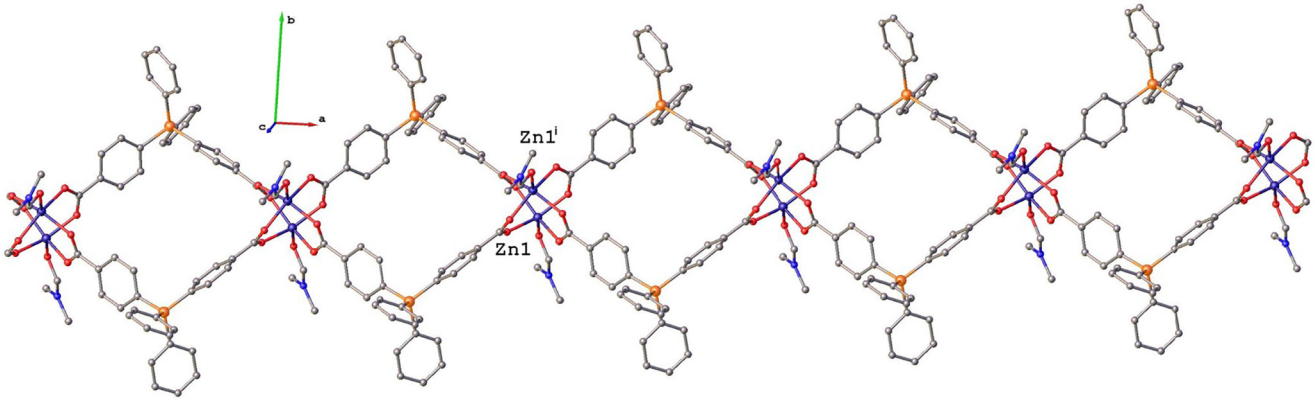


**Fig. 2.** View of the coordination polymer in the crystal structure of **1**. Symmetry code: 1 − *x*, *y*, 1.5 − *z*.

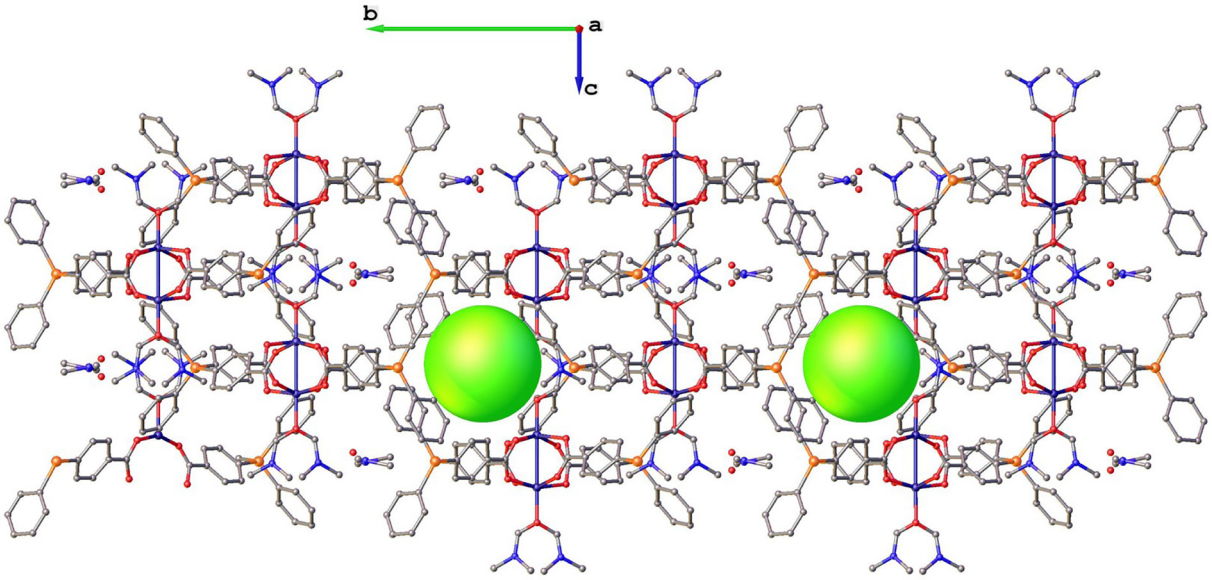


**Fig. 3.** View of crystal structure packing showing the formation of the channels. In two of the channels DMF molecules are replaced by the green spheres. (For interpretation of the references to colour in this figure legend, the reader is referred to the web version of this article.)

lower as compared to those of free $Mn^{2+}$ (960 $cm^{-1}$, and 3305 $cm^{-1}$) [40,41], being indicative of the electron delocalization through coordination. In the case of **1**, the lack of d-d transitions led to the assignment of the 480 nm band to a possible LMCT $d\pi(Zn(II)) \rightarrow \pi^*(L)$ transition.

The fluorescence spectra of the ligand and complexes in crystalline state (Fig. 7(b)) resemble those in solution, being ligand-centered. The red-shifting of the emission peak of complexes is due to the metal coordination to the ligand **L**. The spatial arrangement of the bulky tetraphenylsilane units in crystal prevents establishing any π–π stacking, confirmed by the 9.11(5) Å distance in the co-facial arrangement of aromatic rings in **L**. Therefore, the fluorescence spectra of **L**, **1** and **2** are typical for non-interacting chromophores.

The optical band gap, $E_g$, was estimated by using the DR spectra in the Kubelka – Munk absorbance expression, $F(R_\infty) = [(1-R_\infty)^2]/[2R_\infty]$, where $R_\infty$ is reflectance of the sample with infinite thickness. The power-law relationship of Tauc links the absorption coefficient to the photon energy and the band gap energy [42], so that the Tauc's Equation becames $F(R_\infty) \times h\nu = A(h\nu - E_g)^m$, where m is ½ or 2 for materials with direct or indirect band gap, respectively, and A is a material constant [43]. Extrapolating the linear part of the plot $[F(R_\infty) \times h\nu]^2$ vs. photon energy $h\nu$ (eV) to the energy axis (inset in Fig. 7(c)), the optical band gap of **L**, **1** and **2** have the values of 4.02, 3.97 and 3.40 eV, respectively. The red shift of $E_g$ of metal complexes with respect to that of the ligand can be directly seen by the extended absorption edge of **1** and **2** in the DRS spectra (Fig. 7(c)). This phenomenon, observed in a series of Zn-based MOF's with various dicarboxylic acids as organic linkers [44–46], was interpreted as a direct effect of the electron redistribution between the organic linker and the Zn-cluster [44]. This charge transfer may lower the organic-inorganic interfacial energy, and the decrease in the band gap energy is higher as the size of the Zn-O cluster is greater.

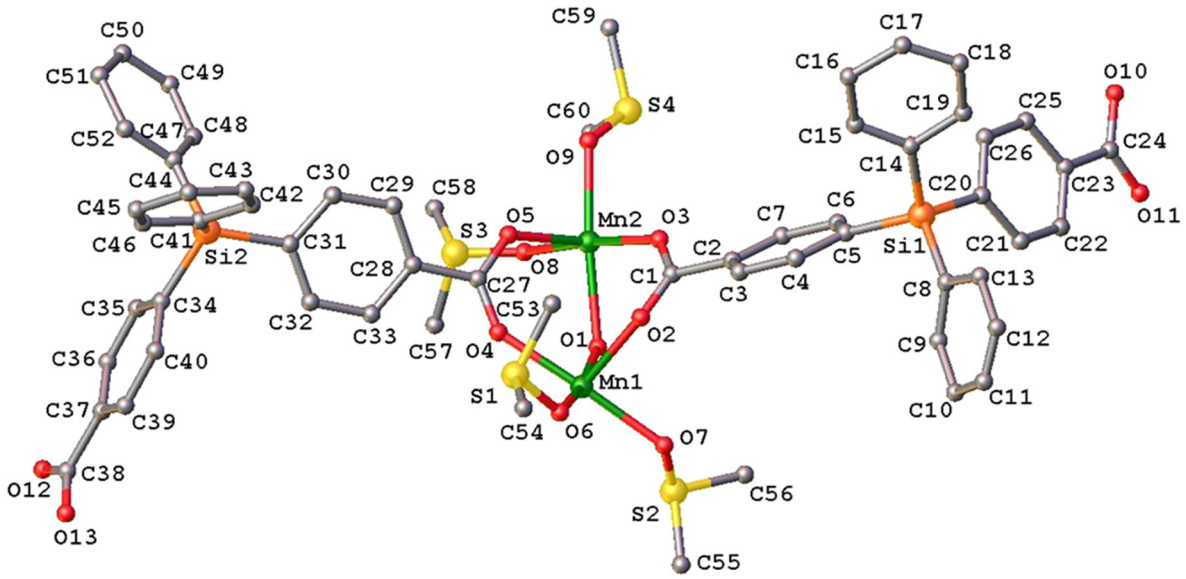


**Fig. 4.** View of the asymmetric part in the crystal structure of **2**. Only the major component of disordered fragments is shown. Hydrogen atoms solvate DMF molecules are omitted for clarity.

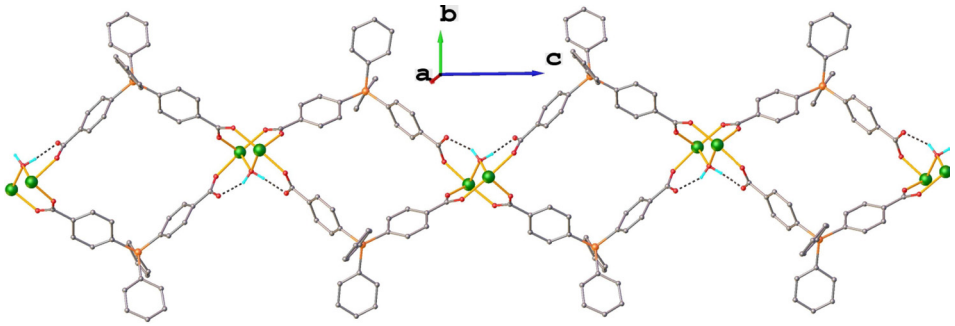


**Fig. 5.** Structure of 1D coordination polymer in the crystal structure **2**. H-atoms, not involved in hydrogen bonding as well as the coordinated and solvate DMSD molecules, are omitted for clarity. H-bonds parameters: O1-H···O10 [O1-H 0.864 Å, H···O10(x, 0.5 − *y*, *z* – 0.5) 1.814 Å, O1-H···O10 2.607(8) Å, O1-H···O10 151.9°]; O1-H···O13 [O1-H 0.862 Å, H···O10(x, −*y* + 0.5, *z* + 0.5) 1.757 Å, O1-H···O13 2.593(8) Å, O1-H··O13 162.8°].

### 3.4. DVS analysis

The design and development of moisture stable coordination polymers is essential for industrial and environmental applications such as water harvesting, desalination, proton conduction, sensing, catalysis, energy storage, gas storage and separation, as well as for $CO_2$ capture [47]. Strategies to increase water stability are addressed to both the relative strength of the metal-ligand bond through the use of tri- or tetravalent metal cations: $Al^{3+}$, $Cr^{3+}$ or $Zr^{4+}$ and the electronic and steric effects of the ligand on the metal node.

The hybrid nature of coordination polymers provides specific building blocks which can be used to target a characteristic behavior of water adsorption. Thus, the structure of the organic ligands, by their hydrophilic/hydrophobic balance and the pore size and pore surface area were found to govern the water stability of coordination polymers. The hydrophobic ligands can protect the inorganic nodes against water coordination or can drive water resistance [48,49], while the introduction of open metal sites and polar groups into the structure by postsynthetic modification is considered to be a major challenge for water sensitivity of certain coordination polymers [50].

Study of water sorption capacity of the Zn(II) and Mn(II) coordination polymers was realized by analysis of the sorption/desorption

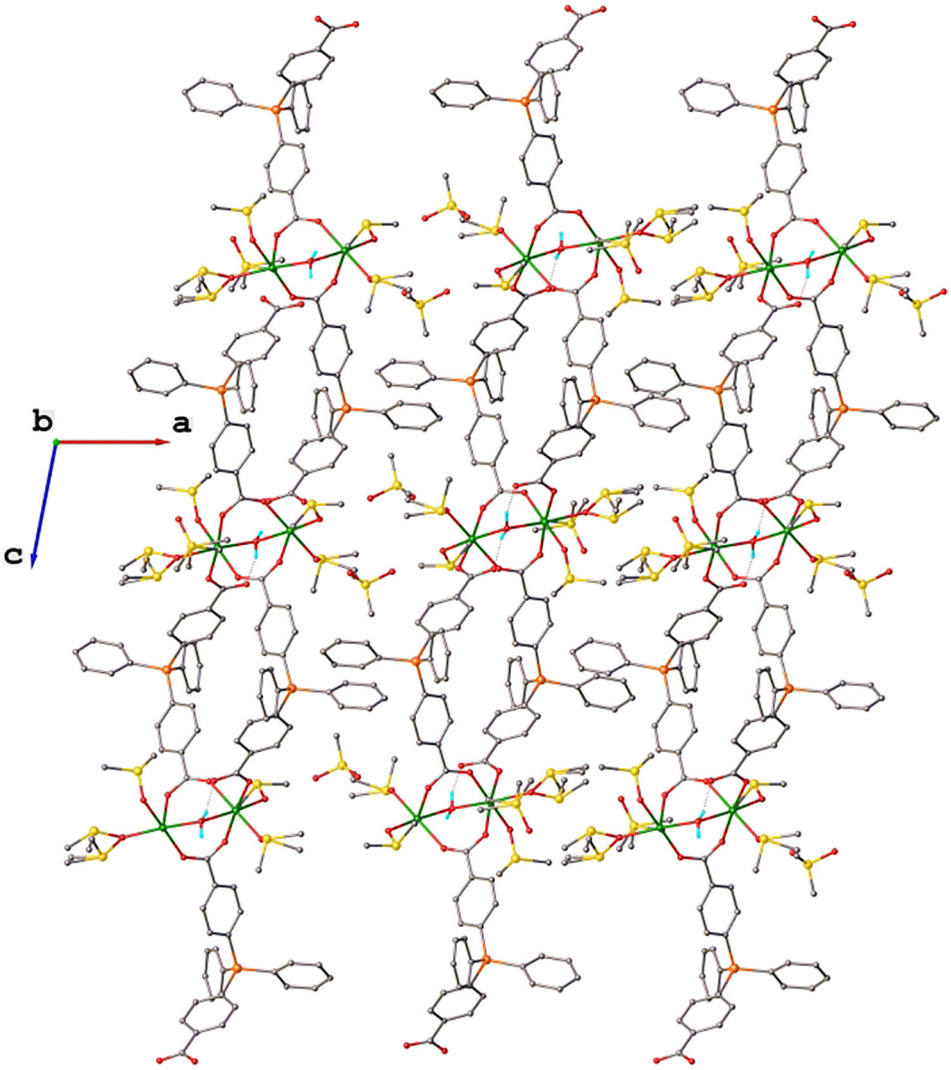


**Fig. 6.** View of the crystal structure 2 along *b* axis.

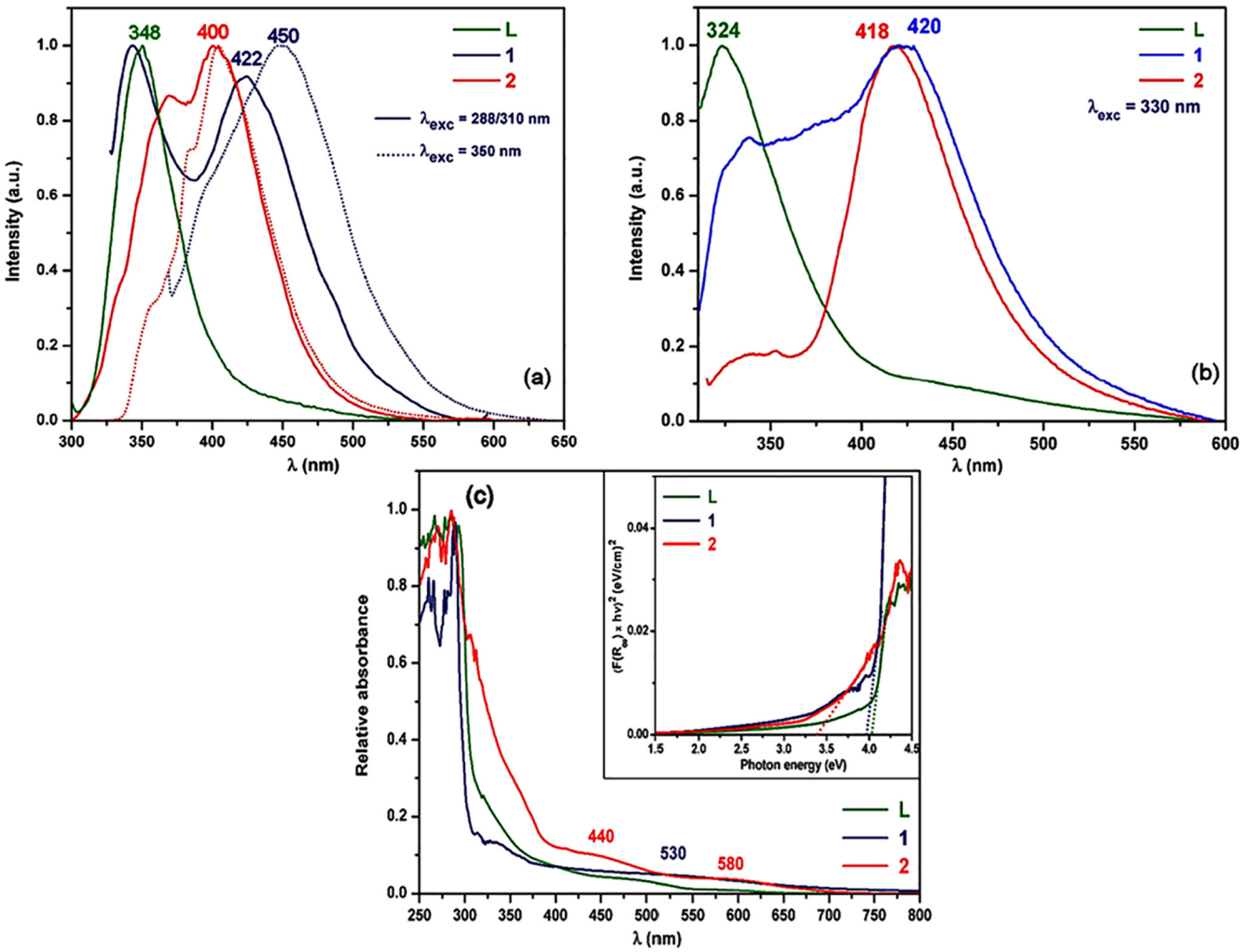


**Fig. 7.** The normalized fluorescence spectra of **L**, **1** and **2** in: (a) DMF solution (c = $1.12 \times 10^{-4}$ M/L); (b) solid state; (c) Normalized diffuse reflectance spectra (DRS) of **L**, **1** and **2** and inset: the Tauc plot of $[F(R_\infty) \times h\nu]^2$ vs. photon energy.

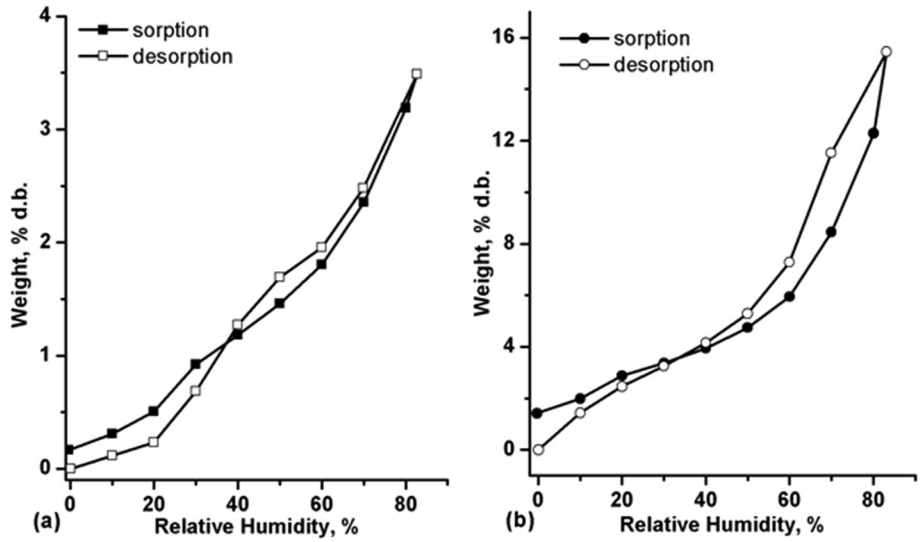


**Fig. 8.** Water vapor sorption-desorption isotherms of: (a)-$\{[Zn_2L_4(DMF)_2]\cdot 0.8DMF\}_n$ and (b)- $\{[Mn_2L_2(DMSO)_4]\cdot 2DMSO\}_n$ at room temperature.

isotherms registered at room temperature. The isotherms recorded are of Type II assigned to a strong physical adsorption followed by a multilayer absorption process [51]. It is known that the sorption process depends on the structural characteristic of the materials as well as on physical ones: temperature, pressure, the relative humidity or exposure time. The structure of the coordination polymers **1** and **2** (Figs. 3 and 5) seems to be responsible of the amount of adsorbed water and the transport of the water molecules in the porous networks. The chemical

structure of the coordination polymers by its dinuclear secondary building blocks and the diphenylsilane-based dicarboxylate ligand are the keys for their performance under moisture conditions. The registered sorption/desorption isotherms of **1** and **2** are present in Fig. 8.

Both the isotherms shape and the sorption capacity values indicate hydrophobic materials with increased hydrophilicity in the case of **2**. The sorption capacity is dependent on their structure: in the compound **1** both carboxylate groups are coordinated in bidentate mode leading to a packing pattern (channels of 8.9 × 11.3 Å) which accommodates solvated guest molecules of DMF (Fig. 3), while in the structure of **2**, two carboxylate groups are coordinated in a bidentate mode and two in a monodentate mode. More than that in the structure of **2** there are coordinated water and DMSO molecules which act as donor/acceptor for adsorbed water molecules (Fig. 5). These specific features determine a higher sorption capacity due to the hydration of the polar groups involved in the hydrogen bonding interactions. The sorption capacity of **1** is 3.49% and 15.45% for **2**. Both samples show a weak hysteresis in the range 40–70 % relative humidity and after the desorption process the samples lose about 0.2% (1) and 0.4% (2) mass due to incompletely removal of guest molecules (Fig. 8).

Based on experimental data of sorption-desorption isotherms, Crank [52] and then Balik [53] have developed different methods to estimate the diffusion coefficients based on second Fick's equation.

So, diffusion coefficient ($D$) can be obtained from a plot giving the ratio of the swollen polymer mass at time $t$ and $t = \infty$ (corresponding to sorption equilibrium), initial slope of a plot of $M_t/M_\infty$ as a function of the square root of time $t^{1/2}$ or limiting slope of a plot of $\ln(1 - M_t/M_\infty)$ vs. $t$ (Fig. 9). At sufficiently *short* times, become determinant the Eq. (1):

$$\frac{M_t}{M_\infty} = \frac{4}{l}\cdot\sqrt{\frac{D_1\cdot t}{\pi}} \tag{1}$$

so: $(M_t/M_\infty)^2 = 16\cdot D_1\cdot t/\pi\cdot l^2 = K_1\cdot t$, where: $K_1 = 16\cdot D_1/\pi\cdot l^2$ result: $D_1 = K_1\pi l^2/16$.

At sufficiently *long* times, become determinant the Eq. (2):

$$\frac{M_t}{M_\infty} = 1-\frac{8}{\pi^2}\cdot e^{-\frac{D_2\pi^2 t}{l^2}} \tag{2}$$

so: $\ln(1 - M_t/M_\infty) = \ln 8/\pi^2 - D_2\cdot\pi^2 t/l^2 = K_2\cdot t$, where: $K_2 = -D_2\cdot\pi^2/l^2$, result: $D_2 = -K_2 l^2/\pi^2$.

As shown in Table 2 the values D1 of the samples **1** and **2** which correspond to short times ($M_t/M_\infty < 0.5$) are less than those of D2 values assigned to long times ($M_t/M_\infty > 0.5$). Both values of compound **1** are smaller than those of compound **2.** The different packing patterns of the structures of **1** and **2** influence considerably the diffusion process. D1 and D2 are higher for compound **2** mainly due to the affinity for water molecules which strongly influence the transport properties and the equilibrium moisture uptake and to the network flexibility.

### 3.5. Thermal analysis

TG/ DTG analysis of the Zn(II) and Mn(II) coordination polymers was performed in the temperature range 25–700 °C, with a heating rate of 10 °C/min, as shown in Fig. 3S and Table 3.

Zn(II) coordination polymer exhibited a first loss of two DMF molecules below 181 °C (11.7% weight loss observed; 12.3% calculated). The next decomposition stages were observed at 343 °C (12.43% weight loss observed; 14.9% calculated) and at 449 °C (36.73% wight loss observed; 38.9% calculated) (Fig. 3S(a)), assigned to the carboxylate groups and aromatic fragments weight loss respectively, with a residual mass of 39.14% corresponding to zinc and silicon oxides (Fig. 4S(a)). Thermal decomposition of the Mn(II) coordination polymer (Fig. 3S(b)) revealed a multiple-step process assigned to the loss of coordinated water and DMSO molecules at 142 °C (12.29%) and 199 °C (6.21%) respectively, to the decomposition of carboxylate groups and aromatic fragments at 300 °C (7.59%) and 466 °C (21.20%). The residual mass of 52.35% correspond ceramic material consisting of metallic oxides formed during thermal treatment (Fig. 4S(b)).

DSC analysis revealed a Tg transition for Zn(II) coordination polymer at 23.86 °C and for Mn(II) coordination polymer at 24.82 °C in the 2nd heating process (Fig. 5S). The presence of the glass transition

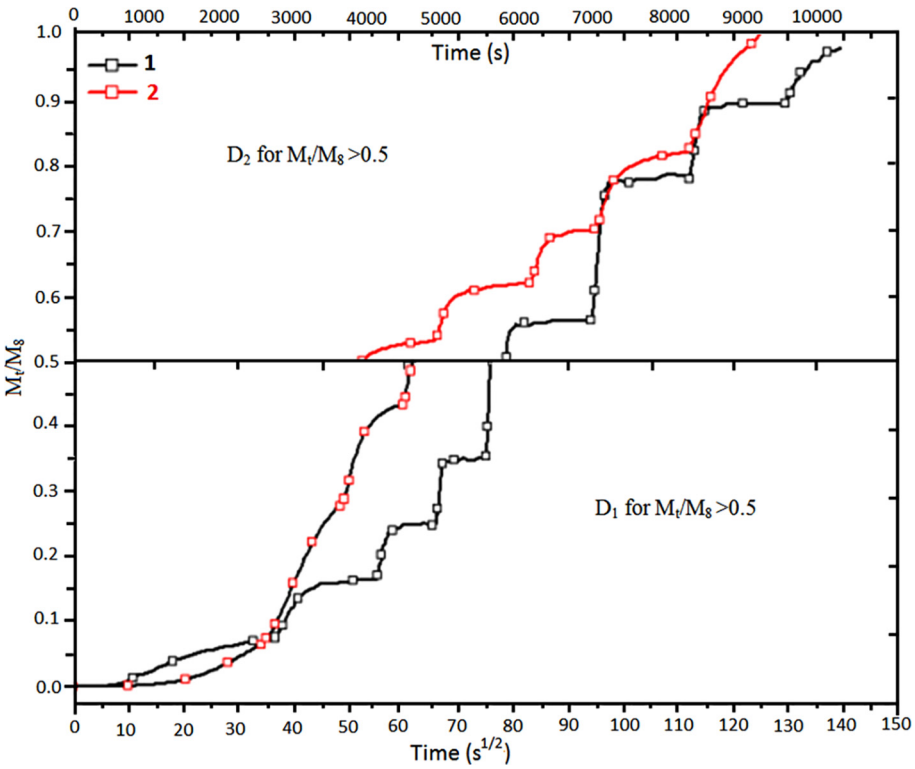


**Fig. 9.** Normalized mass change function of time of compounds **1** and **2.**

**Table 2**
Diffusion coefficients determined from experimental data of sorption/desorption isotherms of **1** and **2**.

| Sample | $K_1^*$, $M_t/M_\infty < 0.5$ | $K_2^*$, $M_t/M_\infty > 0.5$ | *l(cm)* | $D_1 = K_1\pi l^2/16 (cm^2/s)$ | $D_2 = -K_2 l^2/\pi^2 (cm^2/s)$ |
|---|---|---|---|---|---|
| **1** | $5.59{\cdot}10^{-5}$ | $-5.2{\cdot}10^{-4}$ | 0.100 | $1.10{\cdot}10^{-7}$ | $2.27{\cdot}10^{-7}$ |
| **2** | $1.19{\cdot}10^{-4}$ | $-3.16{\cdot}10^{-4}$ | 0.093 | $2.02{\cdot}10^{-7}$ | $2.77{\cdot}10^{-7}$ |

* $K_1$ is slope of linear regression between $(t - t_R)$ and $(M_t/M_\infty)^2$ for $(t - t_R) \geq 0$ and $(M_t/M_\infty)^2 < 0.2$; $t_R$- time correlation (-intercept divided by slope) for $M_t/M_\infty = 0$; $K_2$ is slope of linear regression between t and $\ln(1 - M_t/M_\infty)$ for $1.2 > \ln > 3.0$.

**Table 3**
Thermal characteristics extracted from TG/DTG and DSC curves of $\{[Zn_2L_4(DMF)_2]{\cdot}0.8DMF\}_n$ and $\{[Mn_2L_2(DMSO)_4]{\cdot}2DMSO\}_n$.

| Sample | TGA | | | | | DSC | | | |
|---|---|---|---|---|---|---|---|---|---|
| | Stage | $T_{on}$ (°C) | $T_{max}$ (°C) | $W_m$ (%) | $W_{rez}$ (%) | Scan | $T_g$ (°C) | $T_m$ (°C) | $T_{cr}$ (°C) |
| $\{[Zn_2L_4(DMF)_2]{\cdot}0.8DMF\}_n$ | I | 106 | 181 | 11.7 | 39.14 | 2nd heating | 23.86 | – | – |
| | II | 284 | 343 | 12.43 | | | | | |
| | III | 425 | 449 | 36.73 | | | | | |
| $\{[Mn_2L_2(DMSO)_4]{\cdot}2DMSO\}_n$ | I | 126 | 142 | 12.29 | | 2nd heating | 24.82 | – | – |
| | II | 180 | 199 | 6.21 | | | | | |
| | III | 263 | 300 | 7.59 | | | | | |
| | IV | 396 | 466 | 21.20 | 52.35 | | | | |

$T_{on}$ is the onset thermal degradation temperature determined as intersection point of tangents to the two branches from the beginning of thermograms.
$T_{max}$ is the temperature that corresponds to the maximum rate of decomposition for each stage evaluated from the peaks of the first derivative (DTG) curves.
$W_m$ is the mass loss rate corresponding to $T_{max}$ values.
$W_{rez}$ is the percent of residue remaining at the end of thermal degradation (700 °C).
*Tg* is glass transition temperature.
*Tcr* is crystallization temperature.
*Tm* is melting temperature.

(Tg), characteristic for amorphous polymers or for the amorphous fraction of a crystalline polymer, supports the polymeric behavior of compounds **1** and **2,** because it is well known that at this temperature, portions of the molecules begin to wiggle around and the polymer passes in its rubbery state.

## 4. Conclusions

The self-assembly of bis(*p*-carboxyphenyl)diphenylsilane in the presence of Zn(II) and Mn(II) ions produced 1D linear coordination polymers under solvothermal conditions. In both metallosupramolecular assemblies the packing in the crystal structure occurs with the formation of channels running parallel to *a* crystallographic axis accommodating solvate and guest molecules. Thermogravimetrical data indicated a good thermal stability of both coordination polymers, their polymeric nature being supported by the presence of the glass transition on DSC traces. The water sorption capacity indicated moisture stability of both compounds and a hydrophobic character due to the presence in the structure of the tetraphenylsilane units. The sorption capacity value of Zn(II) coordination polymer was 3.49%, while for Mn (II) coordination polymer was 15.45%, five times higher than Zn(II) polymer, due to its structural peculiarities. From these reasons the estimated diffusion coefficients are found higher for Mn(II) coordination polymer. The photophysical properties of the ligand and of the CPs **1** and **2** were investigated in DMF solution and in solid state, by means of electronic absorption and emission spectroscopy. The violettish – blue emission is originating in the ligand-to-metal charge transfer, although the Zn(II) complexes usually display only the ligand-centered emission. Because the polymers absorption occurs in the UV region, its high transparency beyond 400 nm provides a very suitable basis for its use in optoelectronic devices. The emission in the Visible region is an additional benefit for using the synthesized coordination polymers in designing molecular light-emitting devices.

## Acknowledgements

This work was supported by a grant of the Romanian National Authority for Scientific Research and Innovation, CNCS/CCCDI-UEFISCDI, project number PN-III-P2-2.1-PED-2016-1536 (Contract 130PED/2017), within PNCDI III and by a grant of Ministery of Research and Innovation, CNCS – UEFISCDI, project PN-III-P4-ID-PCE-2016-0642 (Contract 114/2017), within PNCDI III.

## Appendix A. Supplementary data

Supplementary data associated with this article can be found, in the online version, at https://doi.org/10.1016/j.ica.2018.08.027.

## References

[1] M. Yoon, R. Srirambalaji, K. Kim, Chem. Rev. 112 (2012) 1196–1231.
[2] J. Juan-Alcañiz, E.V. Ramos-Fernandez, U. Lafont, J. Gascon, F. Kapteijn, J. Catal. 269 (2010) 229–241.
[3] D.J. Lun, G.I.N. Waterhouse, S.G. Telfer, J. Am. Chem. Soc. 133 (2011) 5806–5809.
[4] X. Lin, N. Champness, M. Schroder, Top. Curr. Chem. 293 (2010) 35–76.
[5] L.E. Kreno, K. Leong, O.K. Farha, M. Allendorf, R.P. Van Duyne, J.P. Hupp, Chem. Rev. 112 (2012) 1105–1125.
[6] M.D. Allendorf, C.A. Bauer, R.K. Bhakta, R.J.T. Houk, Chem. Soc. Rev. 38 (2009) 1330–1352.
[7] J. Hong, L. Huo, Y. Wang, R. Long, C. Zheng, Inorg. Chim. Acta 455 (2017) 81–87.
[8] R.B. Getman, Y.-S. Bae, C.E. Wilmer, R.Q. Snurr, Chem. Rev. 112 (2012) 703–723.
[9] K. Sumida, D.L. Rogow, J.A. Mason, T.M. McDonald, E.D. Bloch, Z.R. Herm, T.H. Bae, J.R. Long, Chem. Rev. 112 (2012) 724–781.
[10] J. Sun, P. Zhang, H. Qi, J. Jia, X. Chen, S. Jing, L. Wang, Y. Fan, Inorg. Chim. Acta 469 (2018) 298–305.
[11] C. Reichenbach, G. Kalies, J. Lincke, D. Lassig, H. Krautscheid, J. Moellmer, M. Thommes, Micropor. Mesopor. Mat. 142 (2011) 592–600.
[12] C.L. White, R.L. LaDuca, Inorg. Chim. Acta 441 (2016) 169–180.
[13] R.-B. Lin, S.-Y. Liu, J.-W. Ye, X.-Y. Li, J.-P. Zhang, Adv. Sci. 3 (2016) 1500434.
[14] S. Keskin, S. Kizilel, Ind. Eng. Chem. Res. 50 (2011) 1799–1812.
[15] Z. Hu, B.J. Deibert, J. Li, Chem. Soc. Rev. 43 (2014) 5815–5840.
[16] B. Liu, J. Mater. Chem. 22 (2012) 10094–10101.
[17] J. Lei, R. Qian, P. Ling, L. Cui, H. Ju, Trends Anal. Chem. 58 (2014) 71–78.
[18] N.S. Panina, A.N. Belyaev, S.A. Simanova, Russ. J. Gen. Chem. 72 (2002) 91394.
[19] A. Karmakar, I. Goldberg, CrystEngComm. 13 (2011) 339–349.
[20] R. Wang, J. Zhang, L. Li, Inorg. Chem. 48 (2009) 7194–7200.
[21] N.L. Rosi, J. Kim, M. Eddaoudi, B. Chen, M. O'Keeffe, O.M. Yaghi, J. Am. Chem. Soc. 127 (2005) 1504–1518.
[22] J. Pasan, J. Sanchiz, C. Ruiz-Perez, F. Lioret, M. Julve, Eur. J. Inorg. Chem. 20 (2004) 4081–4090.
[23] W.H. Bi, R. Cao, D.F. Sun, D.Q. Yuan, X. Li, Y.Q. Wang, X.J. Li, M.C. Hong, Chem.

Commun. (2004) 2104–2105.
[24] Y. Cui, Y. Yue, G. Qian, B. Chen, Chem. Rev. 112 (2012) 1126–1162.
[25] J.B. Lambert, Z. Liu, C. Liu, Organometallics 27 (2008) 1464–1469.
[26] Z. Liu, C.L. Stern, J.B. Lambert, Organometallics 28 (2009) 84–93.
[27] X. Zhao, L. Zhang, H. Ma, D. Sun, D. Wang, S. Feng, D. Sun, RSC Adv. 2 (2012) 5543–5549.
[28] R.P. Davies, R. Less, P.D. Lickiss, K. Robertson, A.J.P. White, Cryst. Growth Des. 10 (2010) 4571–4581.
[29] D. Frahm, F. Hoffmann, M. Froeba, CrystEngComm 15 (2013) 9429–9436.
[30] R.P. Davies, P.D. Lickiss, K. Robertson, A.J.P. White, CrystEngComm 14 (2012) 758–760.
[31] S.E. Wenzel, M. Fischer, F. Hoffmann, M. Froeba, Inorg. Chem. 48 (2009) 6559–6565.
[32] M. Cazacu, A. Vlad, M.F. Zaltariov, S. Shova, G. Novitchi, C. Train, J. Organomet. Chem. 774 (2014) 70–78.
[33] CrysAlis RED, Oxford Diffraction Ltd., Version 1.171.36.32, 2003.
[34] O.V. Dolomanov, L.J. Bourhis, R.J. Gildea, J.A.K. Howard, H. Puschmann, J. Appl. Cryst. 42 (2009) 339–341.
[35] G.M. Sheldrick, SHELXS, Acta Cryst. A 64 (2008) 112–122.
[36] V. Zelenak, Z. Vargova, K. Gyoryova, Spectrochim. Acta A 66 (2007) 262–272.
[37] K. Nakamoto, Infrared and Raman Spectra of Inorganic and Coordination Compounds, fourth ed, Wiley-Interscience, New York, 1986, pp. 203–236.
[38] D. Talapatra, B.K. Mukherjee, Phys. Stat. Sol. B 155 (1989) 541–548.
[39] V. Philip, V. Suni, M.R. Prathapachandra Kurup, M. Nethaji, Spectrochim. Acta A 64 (2006) 171–177.
[40] S. Pandey, R. Kripal, Chinese J. Phys. 52 (2014) 262–271.
[41] D. Mao-Lu, Z. Min-Guang, J. Phys. C Solid State Phys. 18 (1985) 3241–3247.
[42] D.L. Wood, J. Tauc, Phys. Rev. B Condens. Matter Mater. Phys. 5 (1972) 3144–3151.
[43] A. Dolgonos, T.O. Mason, K.R. Poeppelmeier, J. Solid State Chem. 240 (2016) 43–48.
[44] C.-K. Lin, D. Zhao, W.-Y. Gao, Z. Yang, J. Ye, T. Xu, Q. Ge, S. Ma, D.-J. Liu, Inorg. Chem. 51 (2012) 9039–9044.
[45] L.-M. Yang, P. Ravindran, P. Vajeeston, M. Tilset, RSC Adv. 2 (2012) 1618–1631.
[46] R. Ghosh, A.F. Pedicini, P.C. Rao, K.S. Asha, A.C. Reber, S. Mandal, Dalton Trans. 44 (2015) 13464–13468.
[47] P. Li, J. Chen, J. Zhang, X. Wang, Sep. Purif. Rev. 44 (2015) 19–27.
[48] J. Canivet, A. Fateeva, Y. Guo, B. Coasne, D. Farrusseng, Chem. Soc. Rev. 43 (2014) 5594–5617.
[49] C. Racles, S. Shova, M. Cazacu, D. Timpu, Polymer 54 (2013) 6096–6104.
[50] N.C. Burtch, H. Jasuja, K.S. Walton, Chem. Rev. 114 (2014) 10575–10612.
[51] A. Mangel, J. Therm. Anal. Calorim. 62 (2000) 529–537.
[52] J. Crank, The Mathematics of Diffusion, 2nd Ed., Clarendon Press, Oxford, 1975.
[53] C.M. Balik, Macromolecules 29 (1996) 3025–3029.